Leveraging 3D Structure for Robust and Scalable Vehicle Panel Segmentation

Chung-Yu Wei[1]

MSc Data Science and Machine Learning

Industry Supervisor: Dimitri Zhukov

Academic supervisor: Kaan Akşit

September 2025

Abstract

Summarise your report concisely.

Contents

Chapter 1

Introduction

Chapter 2

Dataset

2.1 Overview

The foundation of this project is the **3DRealCar dataset**, an open-source collection of data designed for creating high-fidelity 3D models of vehicles [1]. The dataset is publicly available and can be utilized for commercial purposes, making it an excellent resource for academic and industrial research. It provides a rich combination of 2D images and dense 3D reconstructions of various cars, which is essential for the task of transferring segmentation masks between different views of the same vehicle.

The primary strength of the 3DRealCar dataset lies in its detailed and multi-modal data, captured using a professional 3D scanner. This allows for a precise mapping between the 2D images and the 3D surface of the car, a critical component for our proposed mask transfer pipeline.

2.2 Data Sources and Preprocessing

The success of the projection pipeline is fundamentally dependent on the quality and fusion of several distinct data sources. Each source provides a critical piece of information, from geometric structure to visual appearance. The following subsections detail each data type, its role, and any required preprocessing steps.

2.2.1 Sparse 3D Model (From COLMAP)

The foundational geometric reference for this work is a sparse 3D model generated using the COLMAP Structure-from-Motion (SfM) photogrammetry pipeline [2]. This model is essential for establishing the geometric relationship and coordinate systems between all camera views, providing the camera intrinsic parameters and the precise 3D pose for each image. The model itself is composed of several key files:

`cameras.bin` A database that stores the intrinsic parameters (focal length, principal point, distortion coefficients) for every unique camera model used during the capture process.

`images.bin` This file acts as the primary link between the 2D images and the 3D world. For each image, it records the camera's extrinsic pose (position **tvec** and orientation **qvec**), a list of its detected 2D keypoints, and a crucial list of `point3D_ids` that links each 2D keypoint to its corresponding 3D point.

`points3D.bin` This file stores detailed information for every successfully reconstructed sparse 3D point. Each entry includes its unique `point3D_id`, its precise position (X, Y, Z) in the world coordinate system, its RGB color, and a "track" recording which 2D keypoints in which images observe it.

`points3D.ply` An exported, human-readable version of the data in `points3D.bin`. It stores the XYZ coordinates and colors of all 3D points in the standard Polygon File Format (`.ply`), which can be opened by visualization software like MeshLab to inspect the sparse point cloud.

2.2.2 High-Resolution RGB Images

- **Description**: Standard `.jpg` colour images captured by the primary vehicle cameras.
- **Resolution**: 1920 x 1440 pixels.
- **Role**: These images serve as the **high-resolution visual reference** for the scene. All 2D component masks are defined on these images, and their dimensions provide the target resolution for upsampling other data sources like depth maps.

2.2.3 High-Fidelity Depth Maps

- **Description**: 16-bit grayscale `.png` images captured by a dedicated 3D scanner, where each pixel's value corresponds to a precise distance measurement in millimeters.
- **Resolution**: 256 x 192 pixels.
- **Role**: This dataset serves as the **geometric ground truth** for the vehicle's surface. Its high accuracy is crucial for bypassing the geometric inaccuracies and sparsity of the COLMAP model, forming the basis for the dense projection.
- **Preprocessing**: A critical preprocessing step was to **upsample** these low-resolution depth maps by a factor of 7.5x (from 256x192 to 1920x1440) to match the exact dimensions of the RGB images. This was achieved using **nearest-neighbor interpolation** (`cv2.INTER_NEAREST`) to preserve the integrity of the original depth measurements without introducing artificial intermediate values.

2.2.4 Component Segmentation Masks

The final data source consists of pixel-perfect annotations for 83 distinct vehicle components (e.g., "door_front_left", "bumper_rear"), stored in a COCO-format JSON file. This data defines the precise regions of interest on the source images that are to be transferred and serves as the ground truth on the target images for the final IoU evaluation.

Chapter 3

2D-to-2D Keypoint Matching via 3D Scene Geometry

This chapter presents the methodologies developed for establishing robust 2D-to-2D correspondences between images of a rigid object from different viewpoints. The core challenge in direct 2D matching lies in handling significant changes in perspective, scale, and occlusion. To overcome these challenges, the methods detailed herein leverage an intermediate 3D representation of the scene as a stable, view-invariant bridge. By projecting a point from a source image into this 3D space and subsequently re-projecting it into a target image, a geometrically consistent correspondence can be found. Two distinct approaches are investigated: first, a baseline method employing a sparse 3D point cloud, and second, our primary proposed method that utilises a dense depth map to enable correspondence for any pixel on the object's surface. A detailed analysis of the workflow, mathematical underpinnings, assumptions, and limitations is provided for each method.

3.1 Method 1: Sparse Correspondence using Pre-computed 3D Features

The initial approach serves as a baseline for performance evaluation and is founded upon the sparse 3D reconstruction generated by state-of-the-art Structure-from-Motion (SfM) software. This method is constrained to a sparse set of visually salient feature points identified during the SfM process.

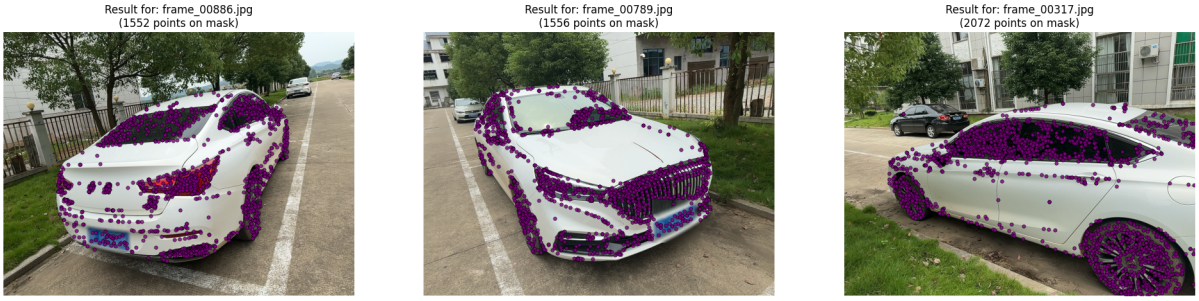

Figure 3.1: Visualization of Sparse Points

3.1.1 Principle of Operation

The fundamental principle is to treat the pre-computed SfM model, specifically the output from COLMAP [2], as a static database. A correspondence is established not by calculating new geometric information, but by querying the existing 3D structure. A known 2D feature point in a source image is used to look up its corresponding 3D point in the model, which is then projected into the desired target view. This process is illustrated in Figure 3.2.

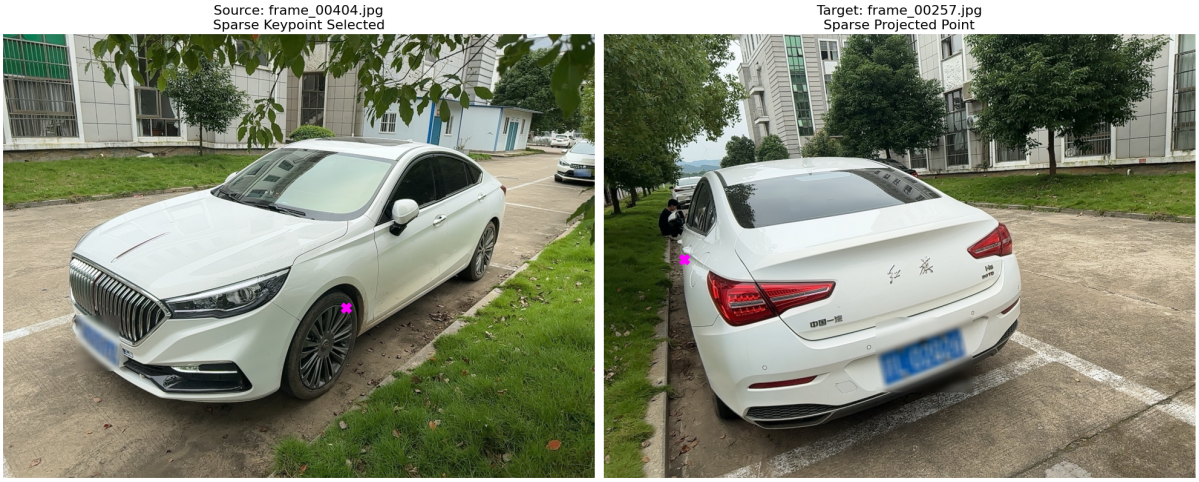

Figure 3.2: Conceptual diagram of the 3D projection pipeline. A point p_s in a source view is back-projected to a 3D point P_w using its depth, then re-projected to point p_t in a target view.

3.1.2 Methodology and Implementation

The execution of this method requires a complete SfM model and a segmentation mask for the object of interest. The workflow is detailed in Algorithm 1.

Algorithm 1: Sparse 2D-to-2D Correspondence

Input: Source image I_s, Target image I_t, COLMAP model $\mathcal{M}$, Vehicle mask M_s

Output: Projected 2D point p_t in I_t

1. Keypoint Filtering:

Let $\mathcal{K}_s$ be the set of all 2D keypoints in I_s from $\mathcal{M}$.

Filter $\mathcal{K}_s$ using mask M_s to obtain a candidate set $\mathcal{K}_{cand} \subset \mathcal{K}_s$ of points on the vehicle surface.

2. Point Selection:

Randomly select a source keypoint $p_s \in \mathcal{K}_{cand}$.

Retain its original index, i, from the COLMAP keypoint list.

3. 3D Position Lookup:

Using index i, retrieve the corresponding 3D point ID, `point3D_id`, from the `images.bin` file in $\mathcal{M}$.

Use `point3D_id` to query the `points3D.bin` file and retrieve the 3D world coordinate P_w.

4. Re-projection:

Let C_t be the camera parameters (pose and intrinsics) for the target image I_t.

Project P_w into the target image frame: $p_t = \text{Project}(P_w, C_t)$.

3.1.3 Assumptions and Limitations

The viability of this method rests on three key assumptions: (i) the geometric accuracy of the camera poses computed by COLMAP, (ii) the rigidity of the vehicle, precluding any deformation between image captures, and (iii) the pixel-level accuracy of the provided vehicle segmentation mask.

The principal limitation is its inherent **sparsity**. Correspondence is restricted to the thousands of salient feature points that COLMAP detects. This method fails for arbitrary user-selected pixels, particularly on texture-deficient surfaces common on vehicles, such as painted panels, windows, or the hood, where no keypoints are likely to exist.

3.2 Proposed Method: Dense Correspondence via Depth Projection

To address the sparsity limitations of the baseline, we propose a dense correspondence method. This technique leverages per-pixel depth information, enabling the projection of any point on the object's surface, not just pre-determined feature points.

3.2.1 Principle of Operation

The core principle is the real-time calculation of a 3D world coordinate for any given pixel. This is achieved by combining the pixel's 2D coordinate with its corresponding depth value, which is retrieved from an aligned depth map. This calculated 3D point is then transformed and re-projected into the target view, establishing a dense correspondence field.

3.2.2 Mathematical Formulation and Methodology

The execution of the dense method relies on the camera parameters from the SfM model and a per-pixel depth map aligned with the source image. The complete mathematical workflow is detailed in Algorithm 2.

Algorithm 2: Dense 2D-to-2D Correspondence via Depth Projection

Input: Source image I_s, Target image I_t, COLMAP model $\mathcal{M}$, Source depth map D_s, Source point $p_s = (u, v)$

Output: Projected 2D point p_t in I_t

1. Depth Retrieval:

Read the depth value d for pixel p_s from the depth map D_s.

2. 3D Position Calculation:

This step computes the 3D world coordinate P_w from the 2D point p_s and its depth d.

(a) Back-projection to Camera Coordinates (P_c): Use the source camera's intrinsic matrix K_s to back-project p_s into the camera's local 3D space.

$$P_c = d \cdot K_s^{-1} \begin{bmatrix} u \\ v \\ 1 \end{bmatrix}$$

(b) Transformation to World Coordinates (P_w): Use the source camera's pose (rotation R_s, translation t_s) to transform P_c into the global world frame.

$$P_w = R_s^T(P_c - t_s)$$

3. Re-projection to Target Image:

This step projects the 3D world point P_w into the target image to find the final coordinate $p_t = (u', v')$.

(a) Transformation to Target Camera Coordinates (P'_c): Use the target camera's pose (R_t, t_t) to bring P_w into the target camera's frame.

$$P'_c = R_t P_w + t_t$$

(b) Projection to Pixel Coordinates (p_t): Let $P'_c = (X', Y', Z')$. Use the target camera's intrinsics K_t to project P'_c onto the image plane.

$$\begin{bmatrix} u' \\ v' \\ 1 \end{bmatrix} = \frac{1}{Z'} K_t \begin{bmatrix} X' \\ Y' \\ Z' \end{bmatrix}$$

3.2.3 Assumptions and Limitations

This method shares the assumptions of camera pose accuracy and object rigidity with the baseline approach. However, it introduces a critical third dependency: **the quality and alignment of the depth map**. The accuracy of the projection is directly contingent on the precision of the depth data and its perfect spatial alignment with the source RGB image.

Several limitations must be noted. First, the method is entirely dependent on the availability of a high-quality depth map. Second, its performance is sensitive to noise in the depth data, which can be significant on specular or transparent surfaces like car paint and glass. Finally, the current formulation does not explicitly handle occlusions; a point visible in the source view may be occluded in the target view, leading to an erroneous projection onto a foreground object.

3.3 Validation: Quantifying Sparse Model Inaccuracy

To provide a quantitative justification for preferring the dense, depth-based approach over the sparse SfM model, a dedicated experiment was conducted to measure the geometric inaccuracy of the sparse reconstruction. This analysis was designed to isolate and quantify the error introduced by the SfM model's geometry, independent of any specific mask transfer task. The findings validate the necessity of the high-fidelity depth maps for achieving precision correspondence.

3.3.1 Experimental Methodology

The experiment measured the re-projection error, defined as the discrepancy between a point's projected position using the sparse model's geometry versus its position derived from the ground-truth 3D scanner data. The process was as follows:

1. **Point Selection**: A 2D keypoint, p_s, detected by COLMAP in a source image was selected. This keypoint has a corresponding 3D point, P_{sparse}, in the global coordinate system of the SfM model.
2. **Sparse Model Projection**: The 3D point P_{sparse} was projected into a designated target camera's view using that camera's pose and intrinsic parameters from the COLMAP model, resulting in a 2D coordinate, $p_{t,sparse}$.
3. **Ground-Truth Projection**: To establish a ground-truth correspondence, we used the high-fidelity depth map. At the coordinate of the original keypoint p_s in the source image, we retrieved its precise, scanner-measured depth, d_{true}. This depth value was used to back-project p_s into a "true" 3D point, P_{true}. This point was then projected into the same target camera's view, resulting in a ground-truth 2D coordinate, $p_{t,true}$.
4. **Error Calculation**: The re-projection error was calculated as the Euclidean distance in pixels between the two projected points in the target image: $E = ||p_{t,sparse} - p_{t,true}||_2$.

3.3.2 Results and Conclusion

The execution of this test across numerous keypoints revealed significant and unpredictable re-projection errors. The error magnitudes frequently exceeded several pixels, with outliers reaching tens of pixels—a level of inaccuracy unacceptable for precise pixel-level tasks like mask transfer.

The analysis confirms that the errors stem not from the projection mathematics, but from the inherent geometric inaccuracies of the sparse SfM model. The primary causes are:

- **Geometric Drift**: SfM reconstructions are known to accumulate small errors in camera poses and 3D point locations. Over a large object, this results in a slight warping or scaling of the model's geometry relative to the metrically accurate ground truth from the 3D scanner.
- **Lack of Surface Constraint**: The sparse feature points are not explicitly constrained to a single, coherent surface and may "float" slightly in front of or behind the true physical surface, leading to large projection errors from novel viewpoints.

This experiment provides the quantitative evidence to support our choice of methodology. It demonstrates that while the sparse model is invaluable for establishing camera poses, its 3D point cloud is not geometrically reliable enough for high-precision correspondence. This result validates the necessity of the dense, depth-map-based methodology (detailed in Section 3.2) for achieving the accuracy required by this project.

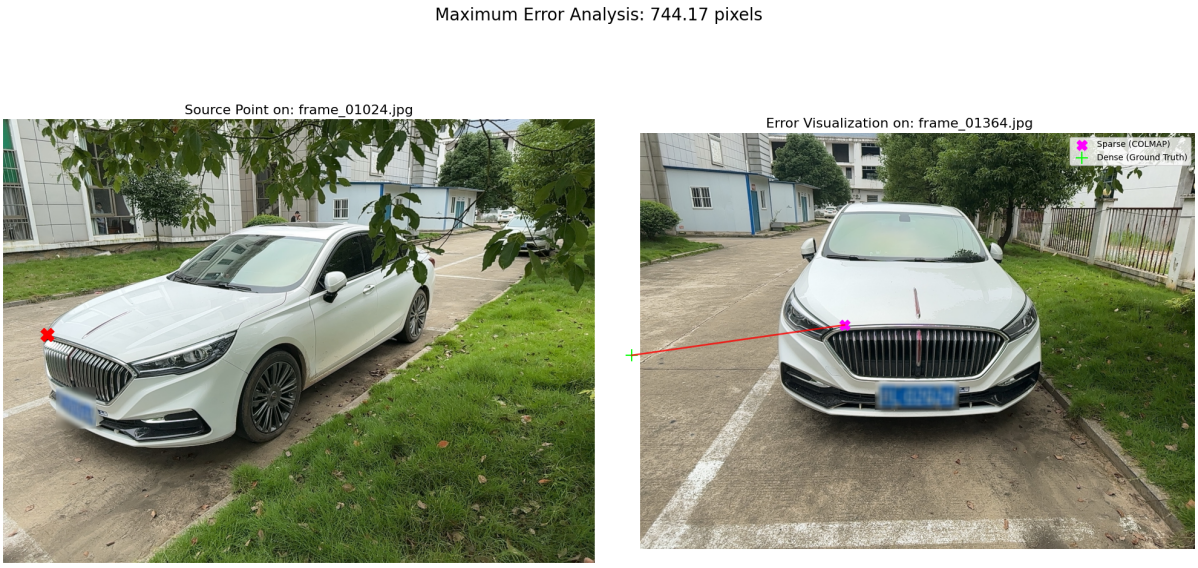

Figure 3.3: A conceptual visualization of the re-projection error analysis. The green dot represent projected locations using the sparse SfM model, while the purple dot show ground-truth locations derived from the depth scanner. The connecting line illustrate the error vector.

Chapter 4

Component mask transfer using dense method

4.1 Introduction

This chapter details the investigation and development of a robust pipeline for transferring two-dimensional (2D) component segmentation masks between different camera views, using a three-dimensional (3D) model as an intermediary. The primary objective is to automate the annotation process by projecting an existing mask from a source image onto a target image with high geometric fidelity.

While the dataset contains annotations for numerous vehicle parts, this work places a specific emphasis on a curated set of components selected for their strategic importance to Tractable's core business operations in automated damage assessment. The accurate and efficient segmentation of these parts is a primary driver for the company's AI-powered solutions. The target components for this study are:

- `bonnet`
- `bumper_f/cover` (Front Bumper)
- `windshield_f` (Front Windshield)
- `headlamp_l_assy` (Left Headlamp Assembly)
- `mirror_l_assy` (Left Mirror Assembly)
- `grille`
- `door_fl_assy` (Front-Left Door Assembly)

The successful transfer of these specific masks is paramount for improving the efficiency and accuracy of automated vehicle inspection.

To achieve this, we developed a dense projection pipeline that was systematically enhanced to address key challenges inherent in 3D-to-2D projection. The pipeline's accuracy was quantitatively validated using two primary metrics: the industry-standard **Intersection over Union (IoU)**, applied when a ground-truth component mask was available in the target view, and a custom **Projection Spread Rate**, which serves as an indicator of projection inaccuracy or significant scale changes between viewpoints. The following sections describe the data prerequisites, the iterative development of the transfer methodology, and an analysis of the results.

The final mask transfer pipeline was developed through an iterative process, starting with a baseline analysis and progressively incorporating more sophisticated techniques to address observed failures.

4.2 V1: A Foundational Dense Projection Method

The V1 pipeline constitutes the foundational implementation of a dense mask transfer. It serves as the most direct and unadulterated application of the projection principle, designed to establish a functional baseline and clearly identify the primary challenges involved in transferring dense pixel regions.

The core methodology of V1 is a "brute-force" projection. For every single pixel located within the boundary of a source component mask, the system uses its corresponding depth value to calculate its precise 3D world coordinate. This 3D point is then immediately projected into the target camera's view. This process is repeated for all pixels in the source mask.

4.2.1 Implementation

The implementation follows a direct, four-step sequence:

1. **Data Preprocessing**: The low-resolution source depth map is upsampled using nearest-neighbor interpolation to match the dimensions of the high-resolution source RGB image and its corresponding component mask.

2. **Point Cloud Generation**: The pipeline iterates through all pixel coordinates (u, v) inside the source mask. Each coordinate is combined with its depth value to back-project it into a 3D point P_w in the world coordinate system.

3. **Direct Projection**: Every generated 3D point P_w is projected into the target image plane, resulting in a list of 2D coordinates (u', v').

4. **Mask Reconstruction**: A blank, black mask is created with the target image's dimensions. The projected 2D coordinates are then "drawn" onto this mask by setting the corresponding pixel values to white.

4.2.2 Results and Critical Limitations

The output of the V1 pipeline is not a solid, usable segmentation mask. As stated in the initial hypothesis and confirmed by experimentation, this direct projection method produces a visually disjointed "point cloud" in the target image. This outcome, conceptualized in Figure 4.1, is a direct consequence of two fundamental flaws.

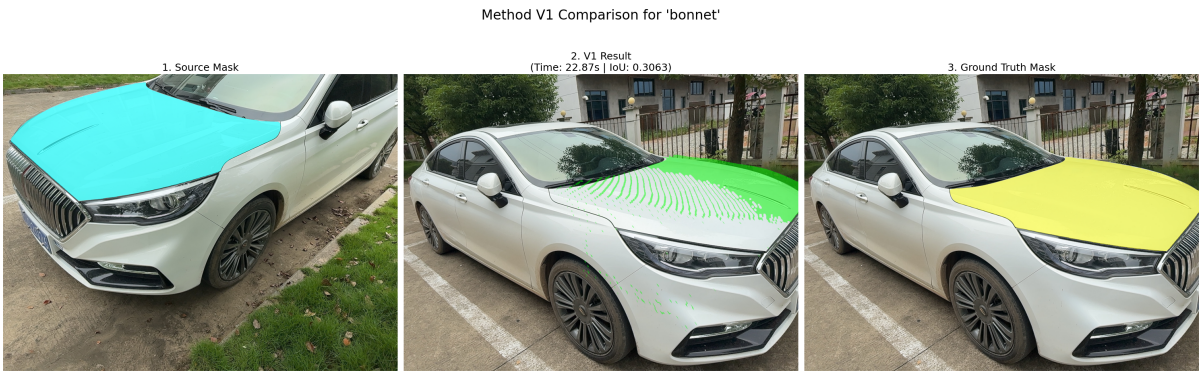

Figure 4.1: Conceptual visualization of the V1 pipeline's output. The direct, raw projection of source pixels results in a sparse and disjointed point cloud in the target image, failing to form a coherent mask.

- **Lack of Surface Continuity**: The primary failure is the inability to produce a solid shape. Due to perspective distortion and the discrete nature of pixel grids, pixels that are adjacent in the

source image are not guaranteed to be adjacent after projection. This results in a sparse output with significant gaps between the rendered pixels.

- **Failure to Handle Any Occlusion**: This simplistic method completely fails to account for perspective occlusions. It lacks any depth-checking mechanism, such as a Z-buffer. As a result, points from the far side of an object are projected just as readily as points from the near side, often appearing incorrectly on top of them. This applies to both self-occlusion and occlusion by other objects in the scene.

In conclusion, the V1 method successfully demonstrates the core concept of dense point transfer but is fundamentally impractical for producing usable segmentation masks. Its clear and predictable failures—the lack of continuity and the inability to handle occlusion—precisely define the essential problems that subsequent versions of the pipeline must solve.

4.3 V2: Geometric Model Fitting for Robust Transfer

The V2 pipeline was developed to overcome the critical limitations of the V1 method, specifically its tendency to distort component shapes and its high sensitivity to noise in the source depth data. The central principle of V2 is to introduce a crucial intermediate step of geometric regularization. Instead of directly projecting the raw, and potentially noisy, 3D point cloud, this method first analyzes the cloud to fit an idealized mathematical model of the component's surface. This clean, geometrically coherent model is then projected, resulting in a transfer that preserves the true shape of the component with much higher fidelity.

4.3.1 Methodology and Implementation

The V2 pipeline is a multi-stage process that incorporates data preprocessing, 3D geometric analysis, and robust projection techniques. The workflow, as implemented in the `transfer_mask_v2` function, proceeds through five distinct steps.

1. **Depth Map Preprocessing (In-painting)**: The process begins by addressing imperfections, or holes, in the source depth map. These are often caused by sensor limitations on specular or transparent surfaces. To create a complete surface for modeling, these holes are filled using the Navier-Stokes based in-painting algorithm provided by `cv2.inpaint`. This technique treats the image intensity as a 2D fluid and propagates information from the boundary of the hole inwards, filling the gap in a physically plausible manner.

2. **3D Point Cloud Generation**: Using the now complete, in-painted depth map, a 3D point cloud $\mathcal{P} = \{p_1, p_2, ..., p_N\}$ is generated by back-projecting every pixel within the source component mask.

3. **Geometric Model Fitting**: This is the core innovation of the V2 pipeline. The raw point cloud $\mathcal{P}$ is processed to create a clean, idealized geometric representation.

   - **For Planar Components (RANSAC)**: For components classified as planar, a **RANSAC (RANdom SAmple Consensus)** algorithm is applied. RANSAC is an iterative, non-deterministic method designed to be highly robust to outliers. The process is as follows:

     (a) A minimal sample of 3 non-collinear points is randomly selected from $\mathcal{P}$.

     (b) These points define a candidate plane with the equation $ax + by + cz + d = 0$.

(c) For all other points $p_i = (x_i, y_i, z_i)$ in $\mathcal{P}$, the perpendicular distance to this plane is calculated. If the distance is less than a predefined inlier threshold ϵ, the point is added to a consensus set.

$$\text{Distance}(p_i, \text{plane}) = \frac{|ax_i + by_i + cz_i + d|}{\sqrt{a^2 + b^2 + c^2}} < \epsilon$$

(d) Steps (a)-(c) are repeated for a set number of iterations. The plane with the largest consensus set (the most inliers) is selected as the final model. This process effectively filters out all noisy depth measurements, yielding a perfectly flat set of inlier points for projection.

- **For Curved Components (Delaunay Triangulation)**: For non-planar components, a **3D Delaunay triangulation** is used to generate a continuous mesh. The Delaunay triangulation has a critical mathematical property: the empty circumsphere condition. For every tetrahedron in the mesh, its circumsphere (the unique sphere passing through its four vertices) contains no other points from the input cloud $\mathcal{P}$ in its interior.

  This property maximizes the minimum angle of all triangles in the mesh, avoiding long, skinny triangles and creating a well-shaped, smooth surface representation. The final set of points to be projected are the unique vertices of this resulting mesh, which captures the component's underlying curvature while averaging out noise.

4. **Projection with Z-Buffering**: The clean set of points from the geometric model (either the RANSAC inliers or the mesh vertices) is then projected into the target view. This process utilizes a Z-buffer to correctly handle self-occlusion, ensuring that only the surfaces visible from the target camera's perspective are rendered.

5. **Final Mask Consolidation**: Even when projecting from a clean model, small gaps can appear in the resulting 2D mask. Therefore, a final morphological closing operation is applied. Using a moderately sized kernel and several iterations, this step consolidates the projected points into a single, solid, and coherent final mask.

4.3.2 Results and Discussion

The introduction of geometric fitting marked a significant improvement in transfer quality. The V2 pipeline produces masks that are far more geometrically faithful and robust to noise than the V1 method. However, its effectiveness remains fundamentally constrained by the quality of the initial point cloud derived from the upsampled depth map.

Figure 4.2 provides a clear case study of the V2 pipeline's performance on the ''bonnet'' component. The method successfully transfers the general location and shape of the component despite a significant change in viewpoint, demonstrating a clear advantage over the V1 method's distorted, "blobby" output.

Despite the improvements, the figure also reveals several characteristic artifacts that highlight the method's limitations. The most noticeable flaw is the "streaky" or "scanline" pattern visible in the transferred mask (Figure 4.2b). This is a direct consequence of the Delaunay triangulation algorithm operating on a point cloud that retains a grid-like structure from the upsampled low-resolution depth map.

Furthermore, the transferred mask exhibits incomplete coverage and small, erroneous flecks of projection noise. These visual inaccuracies are quantitatively reflected in the modest IoU score of 0.4870. While this represents a significant 59% improvement over the 0.3063 IoU achieved by the V1 pipeline, it also highlights the remaining geometric flaws that prevent the method from achieving a higher score.

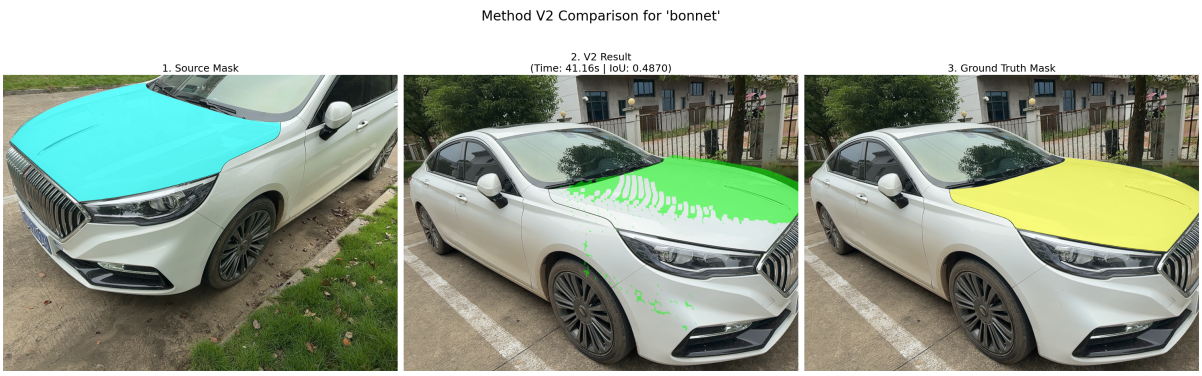

Figure 4.2: A representative result from the V2 pipeline for the ''bonnet'' component. Panel (a) shows the source mask, (b) displays the V2 transferred mask, and (c) provides the ground-truth mask for comparison. The result highlights the method's strengths in perspective handling alongside its characteristic flaws, such as patterned artifacts.

In summary, the V2 pipeline successfully solves the problem of shape distortion and demonstrates a powerful capability for preserving intended geometry. Its key improvements in shape fidelity and noise robustness were a major milestone. However, its performance is still highly dependent on the quality of the input data. Most critically, V2 inherits the fundamental limitation of V1: it fails to handle inter-object occlusions. Its Z-buffer operates only on the component's own geometry and has no knowledge of the wider scene context in the target view. This persistent problem was the primary motivation for the development of the V3 pipeline.

- **Key Improvement: Shape Preservation and Noise Robustness**. By projecting a clean, idealized model rather than raw pixels, V2 excels at preserving the true geometric shape of components. As shown in Figure 4.2, flat surfaces remain flat, and curved surfaces are smooth. The RANSAC and Delaunay steps make the pipeline exceptionally robust to the noisy depth data that plagued earlier versions.
- **Remaining Limitation: Inter-Object Occlusion**. Despite its advancements, the V2 pipeline inherits a critical limitation from V1: it still fails to handle occlusions by other, separate objects in the target scene. Its Z-buffer operates only on the geometry of the component being transferred and has no knowledge of the wider scene context in the target view. Therefore, it will still incorrectly project a mask on top of a nearer, occluding object.

The successful resolution of shape fidelity and noise in V2 was a major milestone. However, the persistent problem of inter-object occlusion demonstrated the need for a final, crucial enhancement: incorporating depth and mask information from the target view itself.

4.4 V3: Full Occlusion Handling via Target Scene Analysis

The V3 pipeline represents the culmination of the single-source transfer methodology, designed specifically to solve the critical problem of inter-object occlusion that limited the V1 and V2 pipelines. While previous versions could handle self-occlusion, they remained blind to the overall geometry of the target scene. The core innovation of V3 is the introduction of a final, decisive visibility check. This is achieved by leveraging the depth map and vehicle mask of the *target* image to ensure that a projected pixel is only rendered if it is physically visible and correctly located on the vehicle's surface.

4.4.1 Methodology and Implementation

The V3 pipeline builds directly upon the geometric fitting framework established in V2. The initial steps of depth map in-painting, 3D point cloud generation, and geometric model fitting (detailed in Section 4.3) are performed identically. The key advancements are introduced in the final projection and masking stages.

1. **Initial Steps (Inherited from V2)**: The pipeline begins by performing the full V2 methodology up to the point of generating a clean, idealized set of 3D points (`points_to_project`) that represents the source component's geometry.

2. **Visibility-Checked Projection**: This step replaces the simple Z-buffered projection of previous versions with a more sophisticated scene-aware analysis. For each 3D point p_{3d} from the idealized model, its visibility in the target scene is determined.

   - The point is first projected to its 2D coordinate (u', v') in the target image. Simultaneously, its depth with respect to the target camera, z_{proj}, is calculated.
   - The ground-truth depth of the target scene at that exact coordinate, z_{gt}, is then retrieved from the target view's high-fidelity depth map.
   - The point is considered visible only if its projected depth is less than or equal to the ground-truth depth of the scene, plus a small tolerance τ_{depth} to account for minor sensor noise and precision differences. The mathematical condition for rendering a pixel is:

     $$z_{proj} \leq (z_{gt} + \tau_{depth}) \tag{4.1}$$

     If this condition is not met, the point is determined to be occluded by a nearer object in the target scene and is discarded.

   This check is the crucial step that prevents masks from appearing on the wrong side of the car or being projected through foreground objects.

3. **Final Masking and Clipping**: The set of pixels that pass the visibility check are rendered onto a raw mask. This mask is then consolidated using the same morphological closing operation from previous versions. As a final step in ensuring physical correctness, the resulting solid mask is clipped using a bitwise AND operation with the target image's overall vehicle mask. This removes any minor projection errors that may have landed just outside the vehicle's silhouette.

subsectionResults and Discussion The V3 pipeline produces the most physically accurate and visually correct masks of any single-source method developed. By incorporating information from the target scene, it successfully resolves the inter-object occlusion problem, which was the primary failure mode of V2.

Figure 4.3 provides a case study of the V3 pipeline's performance, which can be directly compared to the V2 result in the previous section (Figure 4.2). The most notable improvement is the elimination of erroneous projection noise. The small green flecks that were visible on the bumper and wheel arch in the V2 result have been successfully filtered out in the V3 output. This is a direct result of the final clipping step, which performs a bitwise AND operation with the target vehicle's ground-truth silhouette mask, ensuring the final output is strictly confined to the car's body.

Interestingly, this qualitative improvement in cleanliness is not reflected by a major increase in the quantitative score. The V3 result achieves an Intersection over Union (IoU) of 0.4781, a slight decrease from the 0.4870 achieved by the V2 pipeline on the same component. This highlights a key aspect of the evaluation:

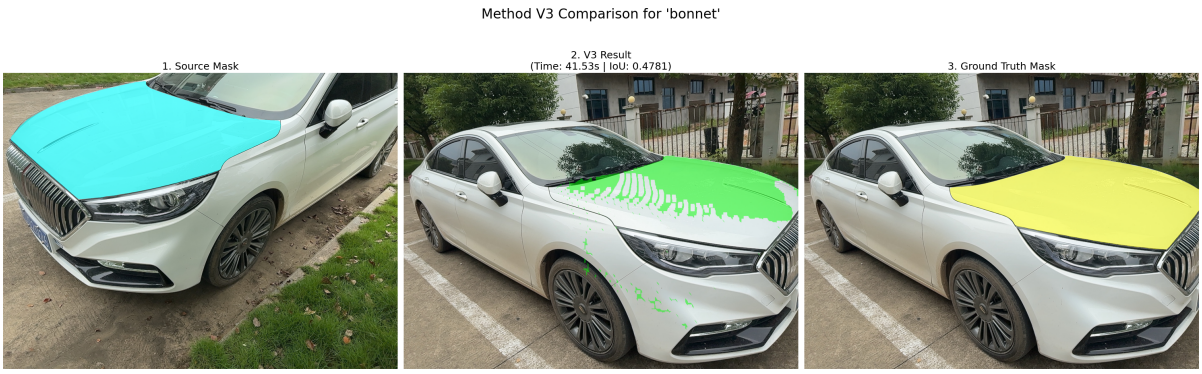

Figure 4.3: A representative result from the V3 pipeline for the ‘’bonnet‘‘ component. The final mask (b) is cleaner than the V2 equivalent, with projection noise outside the main component area removed. This demonstrates the effectiveness of the final visibility check and clipping stages.

- The primary factor depressing the IoU score in both V2 and V3 is the large-scale incomplete coverage caused by the streaky artifacts from the geometric fitting stage (a flaw inherited from V2).
- The noise removed by V3 constitutes a very small pixel area. Removing these few ”false positive” pixels provides a cleaner, more precise result, but it does not fix the much larger ”false negative” area of the missing streaks.

Therefore, the true benefit of V3 is not always a higher IoU, but a significant increase in the physical plausibility and reliability of the output. The resulting mask is more trustworthy, even if the raw score is comparable to V2.

The primary trade-off for this increased accuracy is a significant increase in data dependency. The success of the V3 method is critically contingent on the availability and pixel-perfect accuracy of the depth map and vehicle mask for the target view. This makes the method powerful but less flexible, as it requires high-quality ground-truth data for both the source and target scenes.

4.5 V3-Fast: Optimization via Point Cloud Subsampling

4.5.1 Motivation and Principle

While the V3 pipeline achieves a high degree of physical accuracy, its methodology is computationally expensive. Processing every pixel for large components creates a bottleneck for large-scale applications. The V3-Fast method was developed to address this efficiency problem.

The core principle is that the surface of a vehicle component is often geometrically redundant and can be accurately reconstructed from a fraction of its total surface points. V3-Fast exploits this by introducing a **2D subsampling** step at the beginning of the workflow. The hypothesis is that a significant speedup can be achieved with only a minimal, acceptable loss in accuracy.

4.5.2 Implementation and Mathematical Formulation

The V3-Fast pipeline is a direct modification of the V3 method, introducing a `subsample_step` parameter, n. Instead of processing the full set of source mask pixels, $\mathcal{P}_{src}$, it operates on a smaller, subsampled set, $\mathcal{P}_{sub}$. A pixel (u, v) from the original mask is selected if its coordinates are integer multiples of the

step n. This selection criterion is expressed as:

$$\mathcal{P}_{sub} = \{(u, v) \in \mathcal{P}_{src} \mid u \pmod n = 0 \wedge v \pmod n = 0\}$$

This operation reduces the number of points to be processed by a factor of approximately n^2. The relationship between the number of points before ($|\mathcal{P}_{src}|$) and after ($|\mathcal{P}_{sub}|$) subsampling is:

$$|\mathcal{P}_{sub}| \approx \frac{|\mathcal{P}_{src}|}{n^2}$$

This quadratic reduction in the point cloud size is the source of the dramatic performance gain, as all subsequent computationally intensive steps operate on this much smaller set of points.

4.5.3 Performance Analysis: The Speed vs. Accuracy Trade-off

To determine the optimal subsample step, an experiment was conducted on the seven target components with n values from 3 to 20. The average Intersection over Union (IoU) and processing time were recorded for each configuration.

The results, summarized for the ‘’bonnet‘‘ component in Table 4.1, reveal a clear trade-off. For n values from 3 to 9, processing time decreases exponentially while the IoU score degrades gracefully. Beyond $n = 9$, the IoU drops sharply as the point cloud becomes too sparse for the geometric fitting algorithms to function reliably.

Table 4.1: Performance of V3-Fast on the ‘’bonnet‘‘ component with varying subsample steps (n).

Subsample Step ($n \times n$)	**Average IoU**	**Processing Time (s)**
3x3	0.7450	271.81
5x5	0.7399	89.47
7x7	0.7163	44.02
9x9	**0.7026**	**28.42**
10x10	0.5921	23.97
20x20	0.3386	9.96

In Figure4.4. The data from the experiment reveals a classic speed-versus-accuracy trade-off:

- **Processing Time**: The standard V3 pipeline required **10.93 seconds** to complete the transfer. In contrast, the V3-Fast pipeline finished in just **0.21 seconds**. This represents a massive **52-fold speedup**.
- **Intersection over Union (IoU)**: The V3 method achieved a high IoU of **0.8324**. The V3-Fast method scored a slightly lower but still excellent IoU of **0.7766**. This constitutes a relatively small **6.7% decrease** in the IoU score.

Based on this analysis, a subsample step of $\boldsymbol{n = 9}$ was selected as the optimal parameter. At this value, the pipeline achieves a theoretical speedup of up to **81×** with a relatively minor drop in average IoU, providing the best balance between high-fidelity transfer and computational efficiency.

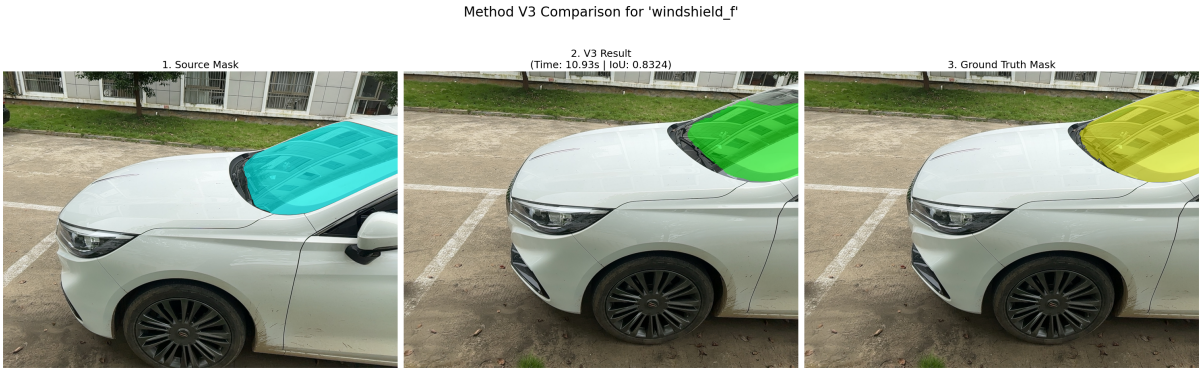

(a) Method V3 Result

(b) Method V3-Fast Result

Figure 4.4: Direct comparison of the (a) V3 and (b) V3-Fast pipelines for the 'windshield_f' component. The images showcase the trade-off between processing time and final IoU score.

4.6 V5: Final Pipeline Tuning and Refinement

4.6.1 Motivation

While the V3-Fast pipeline is computationally efficient, its accuracy is highly sensitive to its fixed hyperparameters, particularly the depth tolerance and morphological kernel size. A strict, small depth tolerance can cause the visibility check to incorrectly discard valid pixels due to minor sensor noise, resulting in undesirable "holes" in the final mask. Conversely, a small morphological kernel may fail to bridge the larger gaps introduced by the subsampling process.

The V5 pipeline was developed to address these issues. It is not a change in the core algorithm but rather the result of a systematic tuning process to find the optimal parameters. The objective of V5 is to maximize the final accuracy and robustness of the transfer by refining the pipeline's hyperparameters and adding critical pre-processing safeguards.

4.6.2 Hyperparameter Optimization and Implementation

Three key aspects of the V3-Fast pipeline were targeted for improvement.

Optimizing Depth Tolerance (τ_{depth})

The visibility check, $z_{proj} \leq (z_{gt} + \tau_{depth})$, is critical for handling occlusions. The tolerance, τ_{depth}, determines how forgiving this check is. A small tolerance is precise but brittle, whereas a large tolerance is more robust to noise but risks incorrectly merging objects that are at different depths.

To find the optimal value, an experiment was conducted on the ‘’bonnet‘‘ component, running the pipeline with various tolerance values from 10cm to 60cm. The results are presented in Figure 4.5.

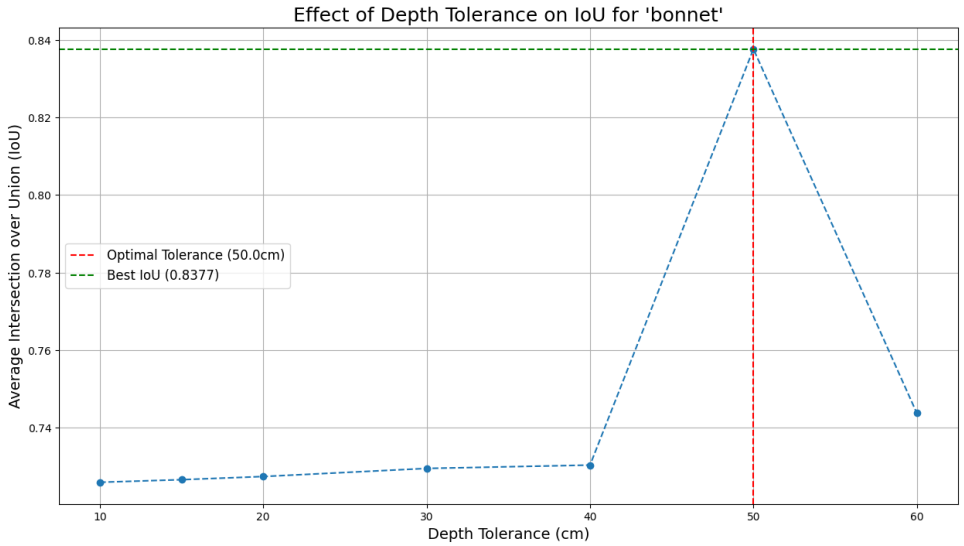

Figure 4.5: The effect of the depth tolerance parameter (τ_{depth}) on the average IoU for the ‘’bonnet‘‘ component. A clear performance peak is observed at 50cm.

The analysis reveals a distinct performance peak, with the maximum average IoU of **0.8377** occurring at a depth tolerance of **50cm**. This value appears to provide the optimal balance, being large enough to overcome typical sensor noise without being so permissive as to cause false merges.

More Aggressive Gap Filling

The ‘9x9‘ subsampling introduced in V3-Fast can create larger gaps between projected points than a denser sampling would. The morphological closing kernel must be sufficiently large to bridge these gaps. Through qualitative analysis, it was determined that increasing the kernel size from ‘7x7‘ to ‘11x11‘ was more effective at producing a single, solid, and coherent final mask without introducing significant shape distortion.

Smarter Source Mask Filtering

To improve the overall reliability of the pipeline, a pre-processing safeguard was added. Before initiating the transfer, a function (`get_mask_size_threshold`) checks if the source mask is large enough to be considered valid. This step prevents the system from wasting computational resources on tiny, noisy, or insignificant source masks that are unlikely to produce a meaningful result, thereby improving the robustness of the entire process.

4.6.3 Final Performance Improvement

The combination of these refinements—a more forgiving depth tolerance, a more aggressive closing kernel, and an intelligent source filter—results in the final V5 pipeline. As shown in Table 4.2, these changes lead to a dramatic improvement in the mean Intersection over Union (mIoU) for key target components compared to the V3-Fast baseline.

For the ‘’bonnet‘‘, the mIoU increased from 0.6252 to 0.8601, a 37.6% relative improvement. For the ‘’bumper‘‘, the mIoU increased from 0.6370 to 0.8069, a 26.7% relative improvement. These results

Table 4.2: Mean IoU comparison between the V3-Fast baseline and the tuned V5 pipeline for key components.

Component	**V3-Fast mIoU**	**V5 mIoU**
Bonnet	0.6252	**0.8601**
Bumper (Front)	0.6370	**0.8069**

confirm that the careful hyperparameter tuning and refinement process in V5 successfully addresses the remaining sources of error, yielding the most accurate and robust pipeline of this study.

4.7 Summary of Methodologies

The iterative development process resulted in several distinct versions of the mask transfer pipeline, each with unique characteristics. Table 4.3 provides a concise comparison of the final five methodologies.

Table 4.3: Comparative summary of the developed mask transfer methodologies.

Method	Description	Pros	Cons
V1	Projects all pixels from the source mask, then uses a Z-buffer and morphological closing.	Simple and relatively fast. Handles self-occlusion.	Can distort shape ("blobby" results). Fails on inter-object occlusion.
V2	Fits a geometric model (plane/mesh) to the source point cloud first, then projects the clean model.	Preserves true geometric shape. Robust to depth noise.	Fails on inter-object occlusion. Can be computationally intensive.
V3	Performs V2, then adds a visibility check against the target's depth map and vehicle mask.	The most physically accurate single-source method. Handles all occlusions.	Requires the most data (target depth & mask). Can be slow.
V3-Fast	An optimized version of V3 that subsamples the source pixels before processing.	Dramatically faster than V3 with minimal loss in accuracy for a given task.	Can lose very fine, single-pixel details due to the subsampling.
V5 (Tuned)	A tuned version of V3-Fast with an optimized depth tolerance, a larger closing kernel, and a source mask size filter.	**Highest accuracy (mIoU)**. Robust to sensor noise, fixing "missing holes." The most reliable and refined pipeline.	Hyperparameters are empirically tuned for the dataset. Retains the high data dependency of V3.

4.8 Analysis of Inaccuracies and Future Improvements

Despite the success of the `v3-fast` and multi-view methods, certain inaccuracies persist. These can be attributed to two main categories: input data imperfections and algorithmic limitations.

4.8.1 Key Reasons for Inaccuracy

- **Input Data Imperfections**: The most significant issue is the **massive resolution mismatch** between the low-resolution ('256x192') depth map and the high-resolution ('1920x1440') image space, which creates "blocky" artifacts. Additionally, **depth sensor noise** on reflective surfaces causes small projection errors.
- **Algorithmic Limitations**: The method's **independent pixel projection** does not enforce surface continuity. Furthermore, the **"brute force" morphological closing** operation is a non-geometric fix that can distort the true shape of a component.

4.8.2 Recommendations for Further Improvements

The most impactful future improvement would be the acquisition of a **better depth map**.

- **Higher Resolution**: A depth map with a resolution closer to the RGB images would provide a near one-to-one correspondence between depth and colour pixels, resulting in dramatically sharper

and more accurate mask transfers.

- **Better Data Completeness**: A higher-quality 3D scanner would be more robust to challenging materials like glass and reflective paint, reducing the number of holes that require in-painting.
- **Higher Accuracy & Less Noise**: A sensor with a higher signal-to-noise ratio would provide more precise depth measurements, translating to smoother, more geometrically correct surfaces and more accurate final projections.

Bibliography

[1] Xiaobai Du, *3DRealCar Dataset*. https://xiaobiaodu.github.io/3drealcar/

[2] COLMAP https://colmap.github.io/tutorial.html

Appendix A

Other appendices, e.g. code listing